LBNL-54927
20-April-2004

Reconstruction of Mechanically Recorded Sound from an Edison Cylinder using Three Dimensional Non-Contact Optical Surface Metrology

V. Fadeyev and C. Haber
Lawrence Berkeley National Laboratory, U.S.A.

C. Maul
TaiCaan Technology, U.K.

J.W.McBride
School of Engineering Sciences, University of Southampton, U.K.

M. Golden

The authors can be contacted at CHHaber@LBL.GOV, VAFadeyev@LBL.GOV, C.Maul@taicaan.com, jwm@mech.soton.ac.uk, mgolden@mitchgolden.com

Abstract

Audio information stored in the undulations of grooves in a medium such as a phonograph disc record or cylinder may be reconstructed, without contact, by measuring the groove shape using precision optical metrology methods and digital image processing. The viability of this approach was recently demonstrated on a 78 rpm shellac disc using two dimensional image acquisition and analysis methods. The present work reports the first three dimensional reconstruction of mechanically recorded sound. The source material, a celluloid cylinder, was scanned using color coded confocal microscopy techniques and resulted in a faithful playback of the recorded information.

1. Introduction

The preservation of mechanically recorded sound is of considerable current interest [1-3]. A recent report [4] demonstrated that certain methods of optical metrology and image analysis could be used to restore mechanical recordings without making contact to the media. These methods also offer the prospect of sampling regions of the surface which have less stylus wear and of reconstructing damaged samples. In this paper we present the first such audio reconstruction using a full three dimensional (3D) measurement of the recorded surface. A 3D measurement is required to reconstruct vertically modulated media such as a cylinder and also to sample the full groove cross section in a lateral recording.

This paper is organized in the following way. The concepts and principles of the method are discussed in Section 2. Section 3 presents a description of the measurement technique. Section 4 describes the analysis and signal processing. The results and prospects are discussed in Section 5 with final conclusions presented in Section 6.

2. Methodology

The reconstruction of recorded sound by image processing has been discussed in some detail already [4]. Here we will summarize the key points and focus on the specifics as regards 3D reconstruction.

In the method, various techniques of electronic imaging are applied to construct a detailed map of the surface structure of a mechanical recording. An example of a 3D image and a cross-section are given in Figure 1. Once these images are acquired analysis techniques can be applied to both emulate the motion a stylus would have made while in contact with the surface and to recover damaged or worn regions. In this way, modern data acquisition and processing capabilities can be brought to bear on the recovery of sound from historical recordings. The aim here is not to (necessarily) provide a real-time playback but rather to extract the maximum information from the sample. The viability of this approach relies upon the use of imaging methods with sufficient resolution and accuracy to sense the minimum undulations of the surface.

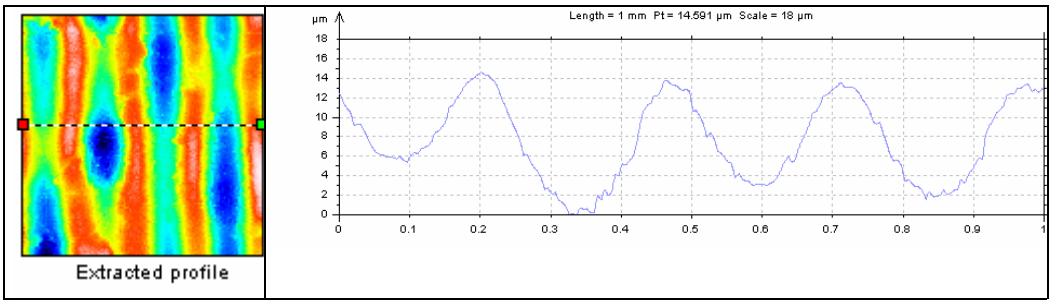

Extracted profile from the altitude measurement

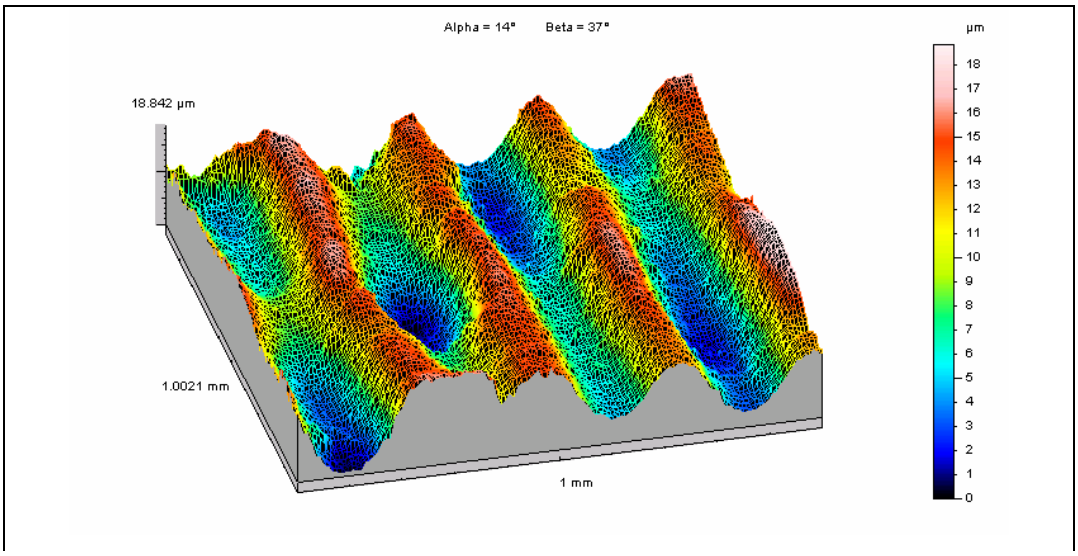

Figure 1: Lower plot shows a 3D surface map of a 1 x 1 mm^2 region of a wax cylinder. Upper plot shown a sectional view across the indicated line. This image was acquired with a CHR450 color coded confocal microscope, manufactured by STIL SA, Aix en Provence, France. The data points were measured on a 6 micron grid, with a 300 micron depth of field probe, at a rate of 4000 points per second. Figure used by permission.

The test of these methods already presented utilized two dimensional (2D) electronic imaging to scan a region of a 78 r.p.m. shellac disc with lateral groove modulation. In that test the groove bottom was readily imaged with an electronic camera and used for the sound reconstruction. To reconstruct media with vertical modulation, such as a cylinder or an Edison "Diamond Disc" 3D imaging is required. This is also the case if the full groove profile in a lateral recording is to be recovered.

Other workers have used optical methods to recover audio from mechanical recordings but these either replace the stylus with a reflected light spot [5-7], reflect light off a low mass mechanical contact [8,9], or are restricted to 2D imaging [10,11]. In the present work, full 3D metrological information is extracted from the surface structure. The general relevance of imaging to the study of cultural artifacts was also discussed by Stanke and Paul [11].

In the methods described here, the physical action of the grooves on a stylus is replaced by a mathematical algorithm executed on digitized surface metrology data. It is therefore important to consider both how the surface structure relates to the audio content, and the surface digitization process itself.

In the case of a magnetic (electrical) recording the playback signal, due to induction, is proportional to the stylus transverse velocity which is due to the lateral groove movement. This proportionality is usually referred to as "constant velocity response", and means that the system-imposed equalization is flat in frequency. Signals are compared on the basis of velocity amplitude rather than power.

$$dB = 20\log\left(\frac{v}{v_{REF}}\right) \qquad (1)$$

where v is the stylus velocity and v_{REF} is some defined reference level (specified in Table A1).

For a sinusoidal modulation, the output signal amplitude will be maximal at the zero crossings of the groove where the stylus velocity is largest. The maximum lateral displacement of the groove corresponding to a zero crossing velocity v_{MAX} is,

$$A_{MAX} = \frac{v_{MAX}}{2\pi f} \qquad (2)$$

where f is the frequency of the recorded tone.

Equation 2 states that for constant stylus velocity (output signal amplitude) the maximum groove displacement depends inversely upon frequency. This condition is inherent to a magnetic stylus. In most electrical recordings the lower frequency sound levels are deliberately attenuated to increase the range of signals which will fit in the groove spacing allocated on a disc surface. In addition, higher frequency sound levels are often boosted to overcome the drop off of Equation 2 and to raise the signals above a high

frequency noise floor. For recordings before the early 1950's this process of equalization was not standardized [12].

Because of the constant velocity response, the time derivative of the groove modulations, in a magnetic recording, will be interpreted as the original sound, with additional modification due to any imposed equalization.

For acoustic recordings, which include all cylindrical samples, the playback signal is approximately proportional to the stylus velocity, but the situation is more complicated than in the magnetic case. The conditions leading to this approximation can be understood from the basic physics of sound propagation, the properties of acoustic horns, and the design of the mechanical sound transducers used in the acoustical recorders and players.

The basic arrangement, used in both recording and playback, is shown in Figure 2. Some sort of a horn or tube is coupled to a diaphragm which either drives (recording) or responds to (playback) a stylus contacting the surface of the recording media. The coupling of the diaphragm to the stylus is through a system of mechanical linkages. The sound, either generated by a source in recording, or received by the listener in playback is a pressure wave. In order for the constant stylus velocity, flat frequency condition to apply, the stylus velocity should be proportional to, and in phase with, the sound pressure at the source/listener at all frequencies. In this case, as in the magnetic one, the time derivative of the surface modulation can be directly interpreted as the sound at the source. This condition is met exactly, only for plane waves [13].

For plane waves, the equation of motion and continuity condition can be expressed, to first order by,

$$\frac{\partial p}{\partial x} = -\rho \frac{\partial u}{\partial t} \qquad (3)$$

$$\kappa \frac{\partial p}{\partial t} = -\frac{\partial u}{\partial x} \qquad (4)$$

where $p = p(x,t)$ is the pressure, $u = u(x,t)$ the velocity, ρ the density and κ the compressibility of the gas. Combining these equations to eliminate either p or u yields the equation for either a velocity or pressure wave traveling at the speed of sound $c = (\rho\kappa)^{-1/2}$ with solutions of the form,

$$p(x,t) = p_M \exp[i(\omega t - kx)] \qquad (5)$$

$$u(x,t) = u_M \exp[i(\omega t - kx)] \qquad (6)$$

where p_M and u_M are constants, ω is an angular frequency and k a wave number. These solutions must obey the condition

$$\frac{k}{\omega} = \sqrt{\rho\kappa} = \frac{1}{c} \qquad (7)$$

which is just the dispersion relation $c = \lambda f$, where $f = \omega/2\pi$ is the frequency and λ is the

wavelength. The coefficients in Equations 5 and 6 are related by $u_M = \kappa c p_M$ and therefore,

$$u(x,t) = \kappa c p_M \exp\left[i(\omega t - kx)\right] \qquad (8)$$

which is the required proportionality and phase relationship for the velocity and the pressure.

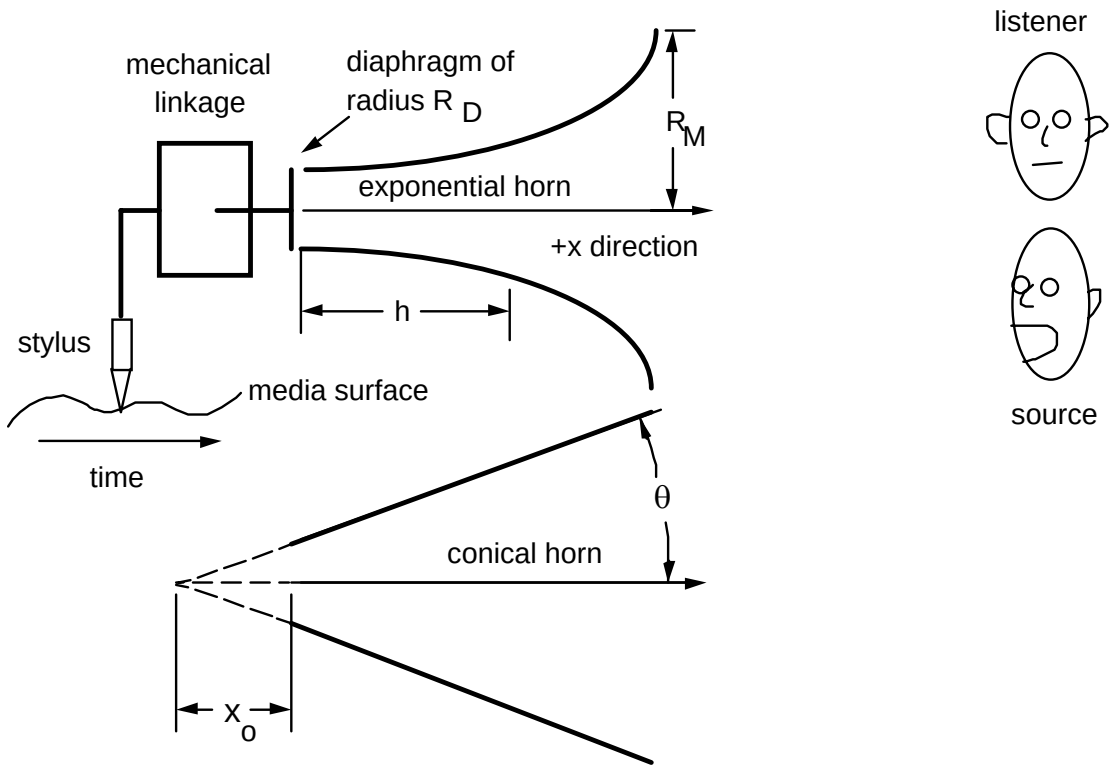

Figure 2: Basic arrangement used in acoustic recording and playback. Shown are two variations of horn, the exponential and conical types, with the same overall length.

The issue is then whether the general arrangement of Figure 2 supports plane waves between the diaphragm and the source or listener [13-18]. For practical reasons, the diaphragm is typically small and therefore not a good transducer for wavelengths $\lambda > 2\pi R_D$, where R_D is the diaphragm radius. For this reason the diaphragm is coupled to the horn which can receive or radiate sound from a much larger effective radius R_M at the mouth end. As long as $\lambda < 2\pi R_M$ the impedance at the mouth end is mostly real and approaches ρc, the free space impedance.

A detailed description of the behavior of horns is complicated and a number of simplifications and compilations have been presented [13-18]. The properties of a horn are equivalent in transmission and radiation. In general, the behavior of a horn is affected by its profile (conical, exponential, catenoidal, etc.) and its length, L. The profile can be described by a cross-sectional area function $S(x)$, where x is position along the axis. In the limit of increasing length and mouth diameter, and/or frequency, the throat impedance of the horn is mostly real and also approaches ρc, meaning that plane waves

are transmitted, and resonances are suppressed. In this limit the horn is a good conduit for plane waves between the throat and the open environment. The use of a horn extends the region of plane wave propagation to lower frequencies than would be possible with just a small diaphragm radiating into an open volume. None-the-less the low frequency response will still degrade at some point and differently so depending upon the horn geometry. At that point the plane wave or constant velocity approximation also breaks down and the time derivative of the surface modulations is no longer precisely proportional to the original sound.

To illustrate this deviation from plane wave response, the finite conical and exponential horns, shown in Figure 2, may be considered as an example. Both will be limited to some overall length L. The conical horn has a opening angle ϑ and an apex distance x_0, such that,

$$S(x) = S_0\left[1+\left(\frac{x}{x_0}\right)\right]^2 \qquad (9)$$

$$S_0 = \pi\left[2x_0 \sin\left(\frac{\vartheta}{2}\right)\right]^2 \qquad (10)$$

The exponential horn has a cross-sectional area function,

$$S(x) = S_0 \exp\left(\frac{2x}{h}\right) \qquad (11)$$

where h is a parameter. The horn transmission coefficient is defined as the ratio of power, introduced by a diaphragm and radiated by a horn of throat area S_0 to that radiated by the same diaphragm, moving at the same velocity, into an infinite cylindrical tube of the same cross-sectional area. The transmission coefficients take the form,

$$\tau_{CONICAL} = \frac{1}{1+\left(\lambda/2\pi x_0\right)^2} \qquad (12)$$

for the conical horn and,

$$\tau_{EXPONENTIAL} = \sqrt{1-\left(\frac{\lambda}{2\pi h}\right)^2} \qquad (13)$$

for the exponential horn. A comparison of these is given in Figure 3 for example horns of the same overall length. The exponential horn has a sharp cut-off at a certain low frequency and a relatively flatter frequency response above cut-off than the conical horn. Where the transmission deviates from unity, the acoustic properties of the horn distort the sound and the constant velocity characteristic fails to apply.

The complete frequency response of the acoustic recording and playback system depends also on the properties of the diaphragm and mechanical linkages. The analysis of Maxfield and Harrison [19] indicates that the purely mechanical transducer acts as a bandpass filter with proper impedance to terminate the horn at the throat up to about 3000-5000 Hz. Below this frequency range the velocity of the diaphragm matches the velocity of the gas. Above this frequency, the mass of the diaphragm limits the response of the system and the transmission of sound again becomes strongly attenuated. If the

horn is not simple, but has bends, additional high frequency limitations may apply as well.

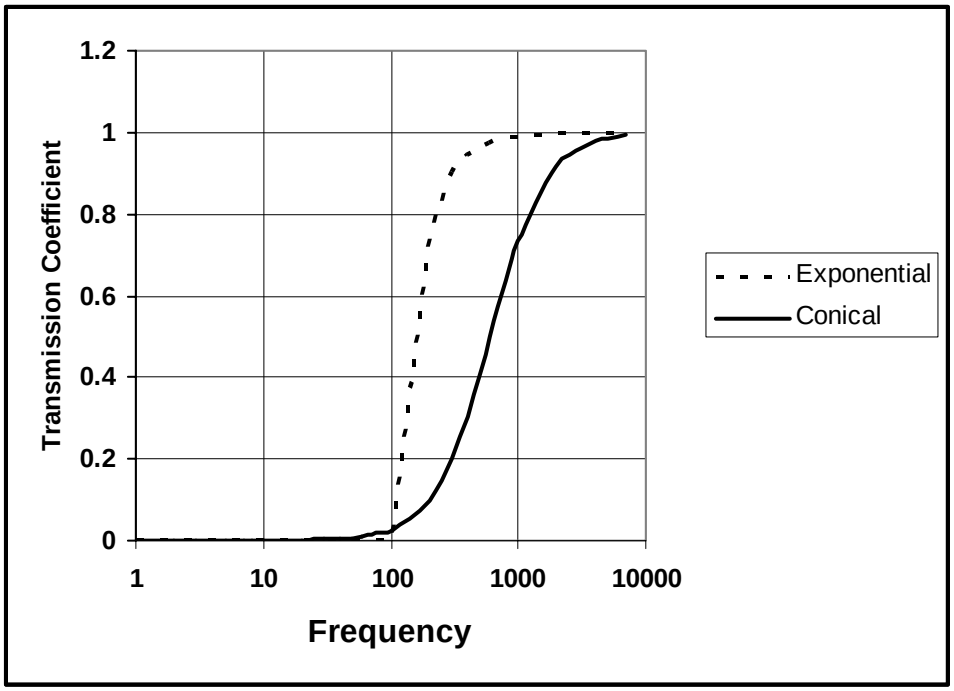

Figure 3: A comparison of the transmission coefficient of an exponential (dashed curve) and conical (solid curve) horn of the same overall length. The particular shapes depend upon the horn geometry but the qualitative trend is characteristic.

Figure 4, from reference [19], shows the frequency response of an advanced acoustic playback system based upon an exponential horn. (See reference [20] for a comment on this plot). The range covered, from 100-5000 Hz, should be considered a best case, benefiting from some of the understanding of horn and transducer properties which emerged late in the acoustic era [21]. There is no evidence to suggest any response above 5000 Hz. The common "rule-of-thumb" [14] was that a horn system could cover only up to one decade in response. The low frequency response of the system discussed by Maxfield and Harrison most certainly benefited from the exponential horn shape to exceed this. Interestingly, many of the archival photographs of studio recording equipment from the acoustic period, show conical horns in use. Figure 5 is an example. If this is typical then these recordings would benefit, in playback, by a low frequency boost which reverses the conical horn response [22]. The one decade "rule-of-thumb" would tend to apply in theses case due to the low frequency roll-off of the conical horn.

A more accurate modeling of the properties of *recording* horns used in the acoustic recording era, and applied to the problem of sound reproduction, could be the topic of a future study. Such models could be used to augment the results presented here. An actual improvement in the recovered fidelity might emerge from such an effort.

From a digitized image of the recording surface, the lateral or vertical displacement of the groove with respect to the un-modulated trajectory is measured on a sequence of points. The measurement of stylus velocity, at each point, is extracted from this displacement

waveform by numerical differentiation. When the constant velocity condition applies, this numerical derivative can be interpreted as the originated sound. Additional low frequency boost can be applied digitally, as a matter of aesthetic judgment, lacking a definite model of the horns used in recording. The resulting data may also be digitally filtered to remove frequencies typically outside the bandpass shown, for example, in Figure 4.

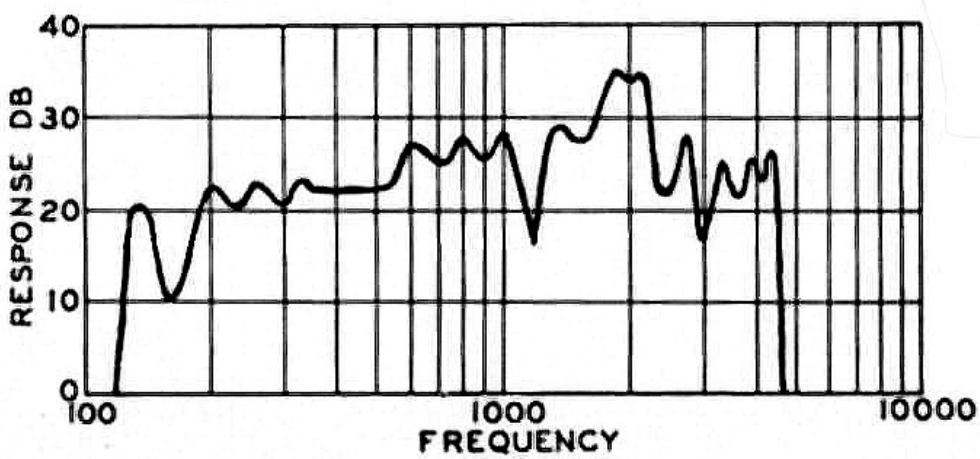

Figure 4: The frequency response of a particular mechanical (playback) phonograph discussed and analyzed by Maxfield and Harrision [19]. (The data shown here was re-plotted by Olsen [17]. See reference [20] for a comment on this.). In this case a folded exponential horn was used, leading to a sharp cut off just above 100 Hz. As discussed, no response is seen above 5000 Hz. The input response of a mechanical recorder of similar construction would be similar as well.

Having established the physical characteristics of the analog recording, the effects and byproducts of digitization may be considered next. A mechanical recording is an analog representation of the source audio waveform. All digital imaging methods acquire object data on a series of discrete points or within discrete pixels. The imaging of the groove pattern is equivalent to a digital time sampling in the spatial direction analogous to time and a digital pulse height sampling in the direction analogous to amplitude. The digital time sampling is determined by the dimensions of the pixel or spot and the spacing between sequential measurements. Let the pixel or spot size be W and the spacing between measured points be D. If $W = D$, the sampling is dense. If W > D the surface is over sampled in that adjacent samples overlap in the direction analogous to time. With a recording linear surface speed S the sampling frequency is given by,

$$f_{SAMPLING} = \frac{S}{D} \qquad (14)$$

In order to satisfy the Nyquist criteria, the digital sampling should be at a frequency at least twice the highest signal tone. In addition, aliasing of higher frequency noise must be avoided. Here there are two possibilities. The sampling could be done at a frequency

sufficiently high that the medium is noise free relative to the baseline noise in the audible range. Alternatively, a low pass filter could be implemented in the primary image acquisition, below the Nyquist frequency, $f_{SAMPLING}/2$. With an imaging element of length $W=2D$ in the time analog direction, groove wavelengths shorter than W will be attenuated according to the filtering function,

$$\sqrt{\frac{2}{\pi}}\frac{\sin\left(\frac{kW}{2}\right)}{k} \qquad (15)$$

Equation 15 represents an imperfect low pass filter for wave number $k < 2\pi/W$ or $\lambda > W$. This corresponds to the frequency $f_{SAMPLING}/2$ and therefore satisfies the Nyquist criterion (to the extent Equation 15 can be considered a low pass filter). This approach requires adjacent time analog samples (pixels or spots) to overlap by D. In this case it may be possible to sample at a lower overall rate at the expense of a more complex imaging and analysis procedure.

Figure 5: Recording at the Edison Studio, 79 Fifth Avenue, New York City, Jacques Urles singing, Sodero conducting, March 30, 1916. Note the narrow conical horn of approximate length 1 meter in use. Photo courtesy of the Edison National HistoricSite, used by permission.

In the direction analogous to amplitude, the measurement system must have sufficient *resolution* and *accuracy* to capture the full range of the audio signal from the intrinsic noise baseline to the maximum groove displacement. Resolution is the smallest change

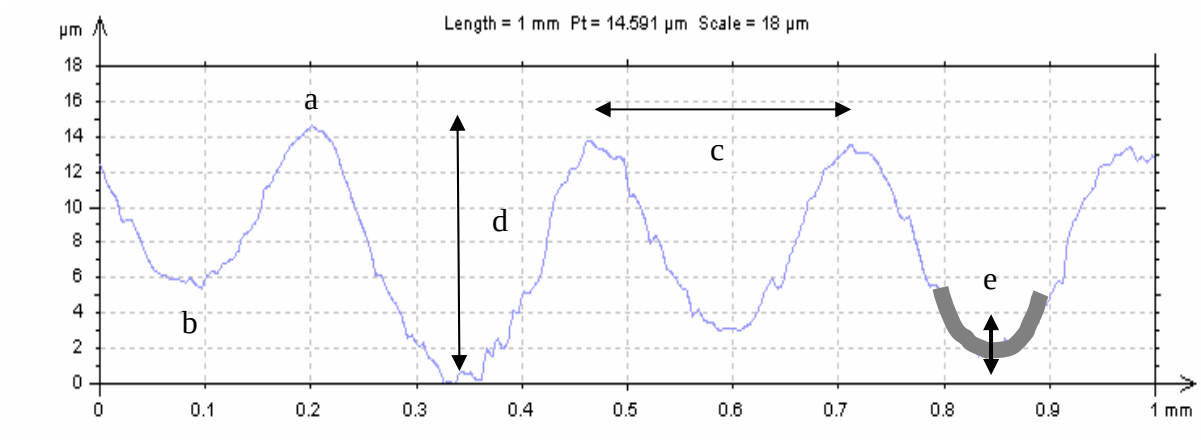

Figure 6: Cross section of Figure 1 showing vertical grooves on the surface of a cylinder. Features are indicated for schematic purposes only: a) ridge between grooves, b) groove bottom or valley, c) groove spacing, d) maximum groove depth, and e) noise is represented by some variation envelope about the groove profile. Horizontal and vertical axes are not on the same scale. Figure based upon Figure 1, used by permission.

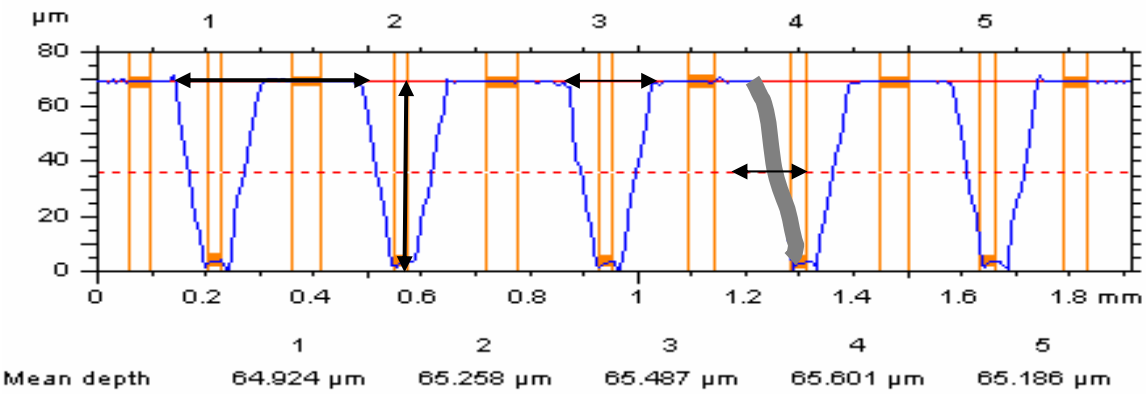

Figure 7: Cross section of lateral grooves on the surface of a disc record. The horizontal arrow between groove 1 and 2 indicates the groove to groove spacing. The vertical arrow in groove 2 indicates the groove depth. The arrow at groove 3 indicated the groove width at the top surface. The grey thick diagonal contour in groove 4 indicates some envelope of variation about the groove profile due to noise, signal, or wear. Note the significant difference between the groove depths here as compared to Figure 3. Horizontal and vertical axes are not on the same scale. Figure (without arrows) is courtesy of STIL SA, used by permission.

in input signal that can be detected. Accuracy is the maximum deviation of the measured value from the true value.

To set the scale, Table A1, of the Appendix, shows the known parameters of mechanical recordings, as determined from a number of sources [23-26]. Figures 6 and 7 relate these parameters to the configuration of grooves on cylindrical and disc media respectively. When relevant they are defined at a specific frequency (1000 Hz) where equalization is generally not applied. Typically the required amplitude measurement resolution will be on the submicron scale.

Methods of high resolution 3D imaging have been developed to serve the need for precision inspection in such fields as semiconductor wafer processing, micro-machining, optics, and paper and fabric processing. Some of the key approaches are based upon either scanning confocal microscopy principles [27,28] or white light interferometry [29,30]. The capabilities of these methods are similar but various trade-offs exist due to speed, cost, and flexibility of measurement.

The basic principle of scanning confocal microscopy [27] is shown in Figure 8. A light source is defined by a pin-hole and brought into focus on the surface of a sample. The reflected light is then refocused on a second pin-hole in front of a photo-detector. The focusing optics are moved and the position corresponding to the maximal detected signal is recorded. As this apparatus is scanned over the surface of a sample the in-focus position of the optics is used to determine the surface topography. Commercial systems feature resolution of 10-100 nanometers, minimum spot sizes of ~1 micron, and data rates of ~1000 Hz. Depending upon the surface quality it may be necessary to average a number of measurements at each point. A variant of this method is shown in Figure 9. For color-coded scanning confocal microscopy [28] a polychromatic pin-hole source is used and the optics has an exaggerated chromatic aberration. Now each wavelength comes into focus at a different depth and the reflected in-focus signal is analyzed by a spectrometer. This method features similar resolution and spot size as the monochromatic approach but may acquire points at a higher rate with stationary optics. Maximum data rates are 4000 Hz and depth of field can vary from 20 μm to millimeters. Figure 1 is an example of an image acquired by this method.

These scanning methods rely also on precision mechanical stages to translate the sample from point to point. If the sample is moving during the measurement the sensor will average over an elongated region of width w (w = *spot size*) and length $l = v/f$ (v=*stage velocity* and f = *data rate*). The minimum time required to scan a region of size *Area* using a grid of points of with spacing g_X and g_Y is given by,

$$T_{SCAN} = \frac{1}{f}\frac{Area}{g_X g_Y} + reset \quad (16)$$

If x is the first scan direction, and the x stage is moving, its velocity v must be fg_X.

As an example, the minimum time required to cover a 2 inch cylinder with g_X = 10 microns, g_Y = 5 microns (a reasonable choice as discussed in below) and f = 4000 Hz is

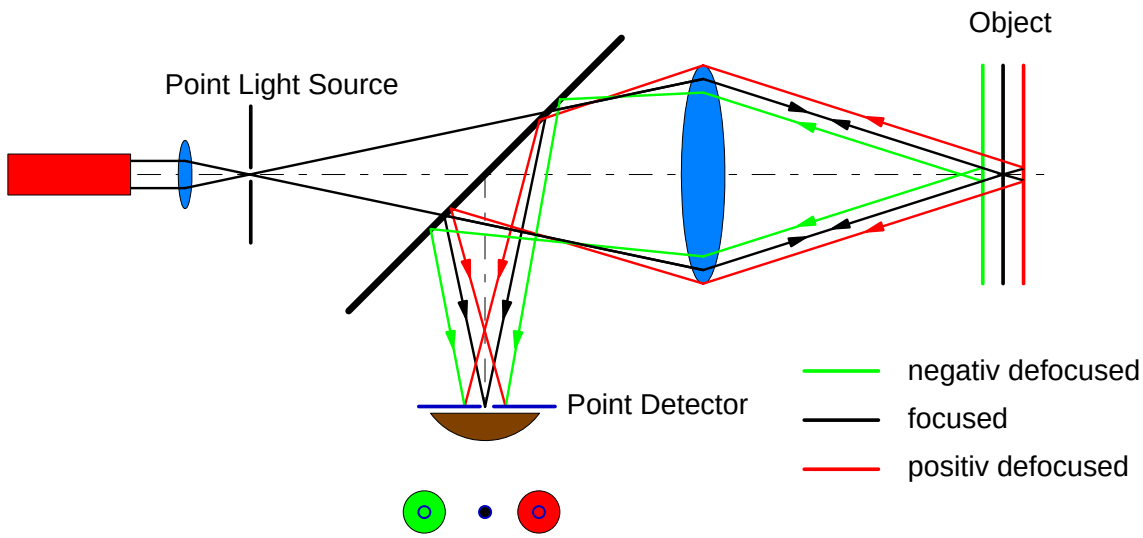

Figure 8: Basic concept of scanning confocal microscopy. The signal in the point detector is correlated with a sweep of the large lens position. Figure is courtesy A.Ruprecht, University of Stuttgart, used by permission.

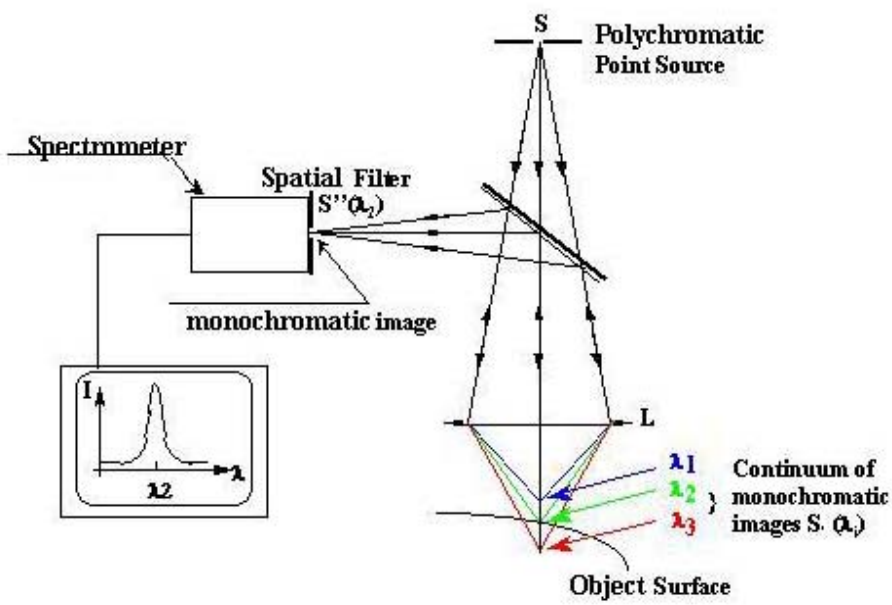

Figure 9: Basic concept of color coded confocal microscopy. The lens at position L has a large chromatic aberration causing the three wavelengths shown to focus at different depths. Figure is courtesy of STIL SA, used by permission.

81000 seconds or 22.5 hours. Factors of 2 or more improvement come with a coarser grid size if allowed. In practice it may be necessary to stop and start the scan periodically in order to control positioning systematics, re-establish a home position, or gather data. In this case an extra term (*reset*) should be added to Equation 16 to account for this overhead.

The basic principle of white light interferometry is shown in Figure 10a. A white light source is used in order to maintain a short coherence length and to localize the interference fringes to the narrow envelope shown in Figure 10b. The system is then configured as, for example, a Michelson Interferometer (or alternate). Light reflected from the sample is combined with that reflected from the reference mirror at the focal plane of a Charge Coupled Device (CCD) or other pixelated imaging array. As the sample, or the interferometer, is scanned along an axis, perpendicular to the sample surface, a series of fringes evolve on the image plane. Coincidentally, a series of image frames is collected and then processed to recover surface structure. The number of planes required, and the spacing between planes, is determined by the slopes and height differences on the sample. This method can image an entire area at once of size determined by the usual constraints of 2D imaging; field of view (FOV), magnification, pixel geometry, and required transverse resolution in the plane. The vertical resolution of this method is typically 10 nanometers. The image acquisition time is determined by camera frame rates, the number of frames per view required, and scanning overhead such as step-and-repeat shift and settling times. For a surface with continuous variation, like mechanically recorded media, typically 1 – 15 seconds is required per view depending upon depths and slopes.

An example of WLI measurement of the surface of a black wax Edison cylinder is shown in Figure 11. That image was acquired with a Veeco Instruments NT1000 WLI system using a magnification of 2.5x for a pixel size on the sample of 3.96 microns. The time required to measure the field was t_{MEAS}=7 seconds. Higher performance versions of these systems exist. The Veeco Instruments NT8000 can scan the same field in t_{MEAS}= 1-2 seconds.

To cover a large surface of size = *Area*, the measurement would be repeated on a regular pattern and adjacent processed images stitched together. The minimum time required to cover the region is determined by the FOV, t_{MEAS}, and the time required to *shift* to the next position.

$$T_{SCAN} = \frac{Area}{FOV} t_{MEAS} + shift \qquad (17)$$

The FOV, combined with the pixel size will determine the transverse resolution of the measurement. As an example, to cover the surface area of a cylinder, as given in Table A1, with a pixel size projected onto the surface of the same 3.96 microns requires a FOV=1.8 x 2.5 mm, With t_{MEAS}= 2 second, and *shift*=0, the minimum T_{SCAN}= 2 hours. To cover the surface area of 10 inch shellac disc recording is correspondingly longer due to surface area and groove depth (Table A1), typically 4-7 hours, minimum. Factors of 2 or more improvement can be made with larger FOV but the absolute required resolution would have to be determined.

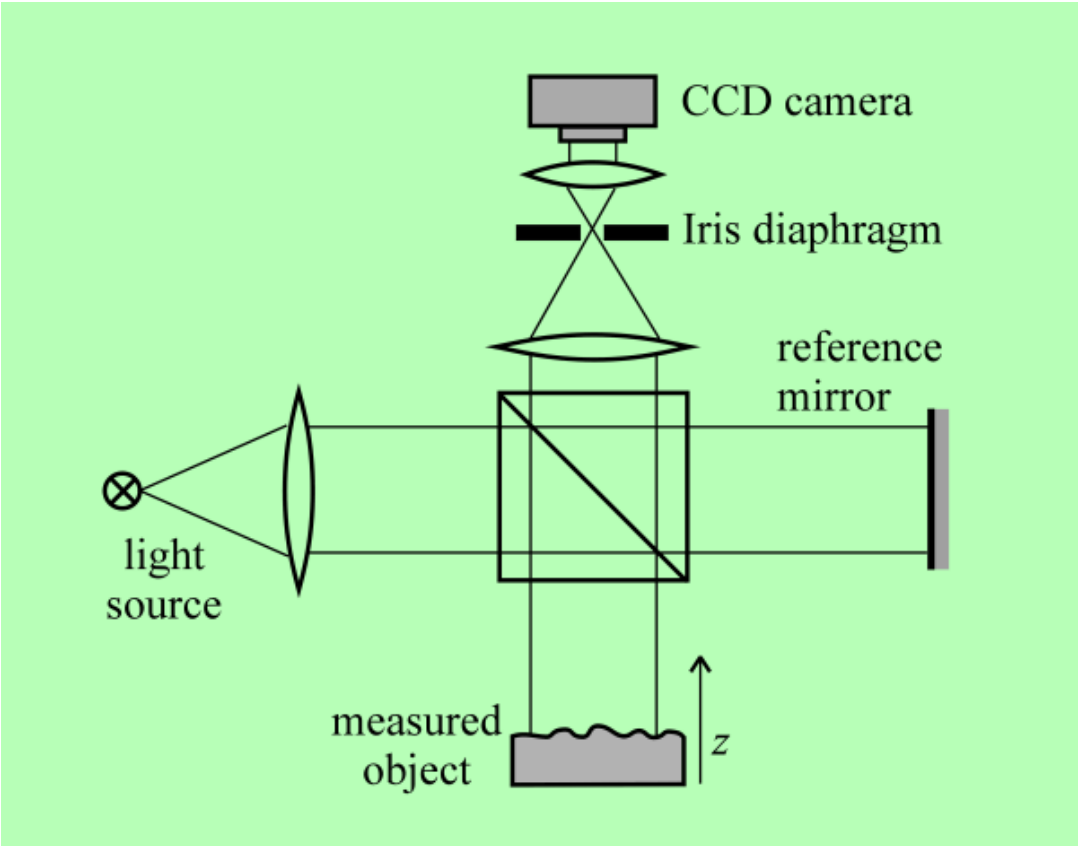

Figure 10a: Basic concept of white light interferometric surface measurement. As measured object moves in indicated z direction the fringe pattern on the CCD camera evolves. Due to the short coherence length of the white light it is not necessary to count fringes. For each pixel on the CCD the envelope shown in Figure 7b is determined as a function of z position. Figure courtesy P. Pavlicik, RCO Czech Republic, used by permission.

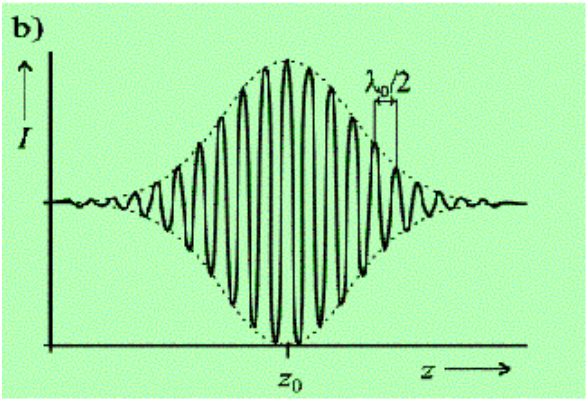

Figure 10b: Amplitude of interference pattern seen in each pixel of Figure 7a. Figures are courtesy of Veeco Instruments Inc.

Frame rates in the WLI approach, and sensor rates in the confocal scanning approach are fundamentally limited by the reflected light from the sample. Improvements can come with brighter light sources, more sensitive photo-detectors, faster frame rate cameras, and more sophisticated motion control systems. The commercial motivation driving further developments is large area, high resolution inspection for flat panel displays, wafers, micro-electrical and mechanical devices (MEMs) and other technologies. Due to the value of these markets improvements are to be expected.

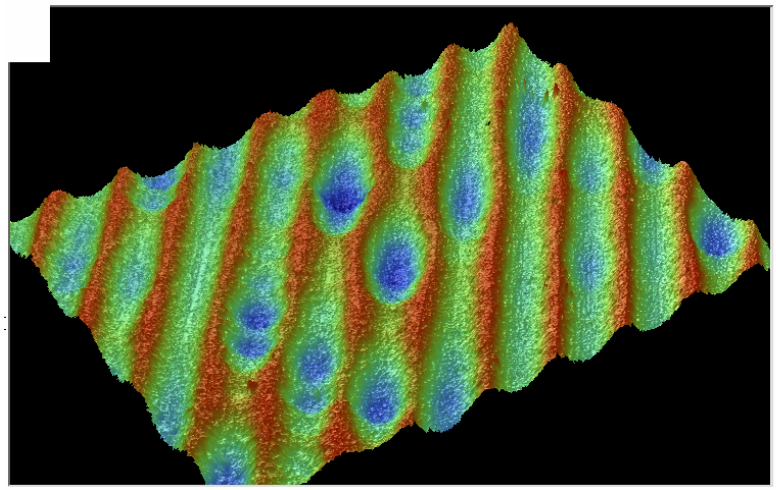

Figure 11: Example of an image field acquired with the Veeco NT1100 white light interferometry system. Image is from surface of a black wax cylinder. Figure is courtesy of Veeco Instruments

The confocal and WLI imaging methods also present different approaches to the low pass filtering strategies discussed in relation to Equation 15. In the confocal case the spot is is conveniently elongated if the faster scan direction is parallel to the time axis on the media. To achieve the low pass filter effect each position needs to be scanned twice with a half-step shift between. In the WLI case each field would be imaged twice with a half pixel offset between. In some custom implementation the WLI imager could be designed with rectangular pixels projections in order to optimize this.

Table 1 compares the confocal and white light imaging approaches.

Table 1: Comparison of confocal and white light imaging technologies.

Parameter	**Confocal**	**White Light Interferometry**
Acquisition	Circular or elongated point	Pixel field n x m elements
Transverse resolution	1.5 - 10 μm	Projected pixel size 1-10 μm
Vertical resolution	10 nanometers	10 nanometers
Points/measurement	1	n x m ~ 480 x 540 = 259200
Max Time/measurement	250 μs	1-10 seconds
Effective time/point	250 μs	4-40 μs
Low pass filtering?	Two passes with offset	Image field twice with offset
Depth of field	20 μm – millimeters	Depth is scanned
Cost of probe only	~$30K	>$100K

3. Measurement Process

In the study described here the color coded confocal imaging method was used because it was available and already in practice by the authors. As discussed in Section 2, the parameters which can vary in such an approach include the size of the point, the depth of field, the resolution, the data rate, and the spacing between points in a scan. In the case of a mechanical recording, the point spacing along the groove direction determines the ultimate sampling frequency. The spacing across the groove contributes to the accuracy with which the groove profile position can be determined at any one time slice.

The Model CHR150 probe, manufactured by STIL SA, was used here. This probe was coupled to custom configured stage movement and read out through a computer. The stages were controlled by DC servo motors and read out by linear encoders. The linear stage resolution was 100 nanometers and the accuracy was 2 microns. The operating characteristics of the scanner and stage movement used are listed in Table 2. The setup is shown in Figure 12.

Table 2: Parameters of the confocal probe used in this study.

Parameter	**Value**
Probe Model	STIL CHR150
Depth of field	350 microns
Spot size	7.5 microns
Sampling Frequency	300 Hz
Vertical Resolution	10 nanometers
Vertical Accuracy	100 nanometers
Step size across grooves	10 microns
Step size along grooves (circumferential)	0.01^{o} (= 5 microns on circumference)
Linear scan speed (parallel to cylinder axis)	3 mm/second

The sample studied was an Edison Blue Amberol cylinder and is described in Table 3. The artist is shown in Figure 13.

Table 3: Description of the cylinder sample studied here.

Parameter	**Value**
Cylinder issue	Edison Blue Amberol
Diameter	2 inch (2.1875 inches)
Artist	Will Oakland and Chorus
Title	“Just Before the Battle, Mother”
Serial number	1516 (..76; 4M-297-2) originally as Amberol #297 1909
Date of original recording	1909
Date of manufacture	~1920’s
Tracks per inch (t.p.i.)	200
Groove spacing	127 μm

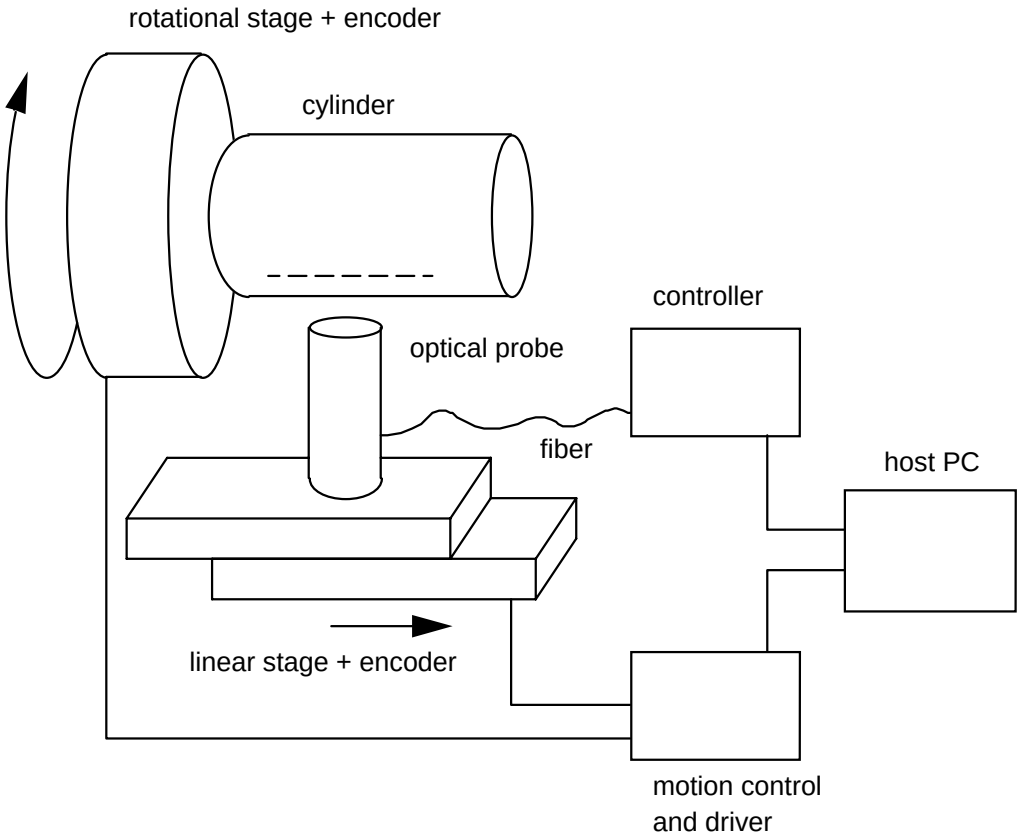

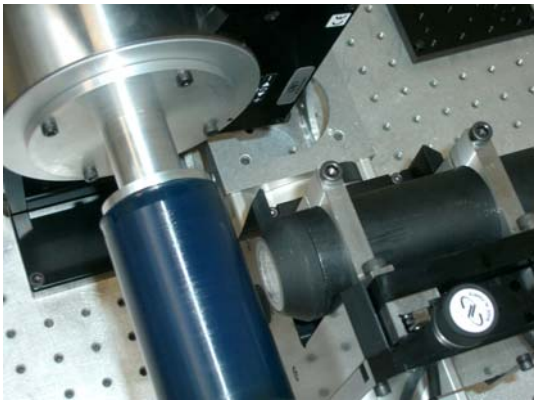

Figure 12: Top imaged is a schematic view of the scanning apparatus.. Lower left image shows overall setup including linear and rotational stages. In lower right image, confocal probe enters diagonally from the center right. Cylinder enters diagonally from the bottom center.

The surface scanning strategy used was based upon the parameters of the probe and the recording. As a matter of convention, “lateral” will refer to the direction across the tracks and parallel to the axis of the cylinder. As a matter of convention, “temporal” or “azimuthal” will refer to the direction along the tracks. The result of a cylinder scan will be a data set consisting of heights at various lateral and azimuthal positions. From the lateral point set at each azimuthal (temporal) position, a best estimate of the track depths can be derived. The lateral sampling interval is determined such that sufficient accuracy is found on the track depth. The azimuthal or temporal sampling is determined to provide for sufficient audio sampling.

Figure 13: Will Oakland

For the 200 t.p.i. cylinder technology of the present sample, the groove width is 127 microns ridge to ridge. The confocal probe spot size used is 7.5 μm and the probe signal averages over a region of width 7.5 μm and length fg_X during a single measurement. Sufficient points must be acquired across the profile to assess its shape. For the 127 micron pitch, 10 microns between points per was judged sufficient assuming complex damage structures did not need to be resolved.

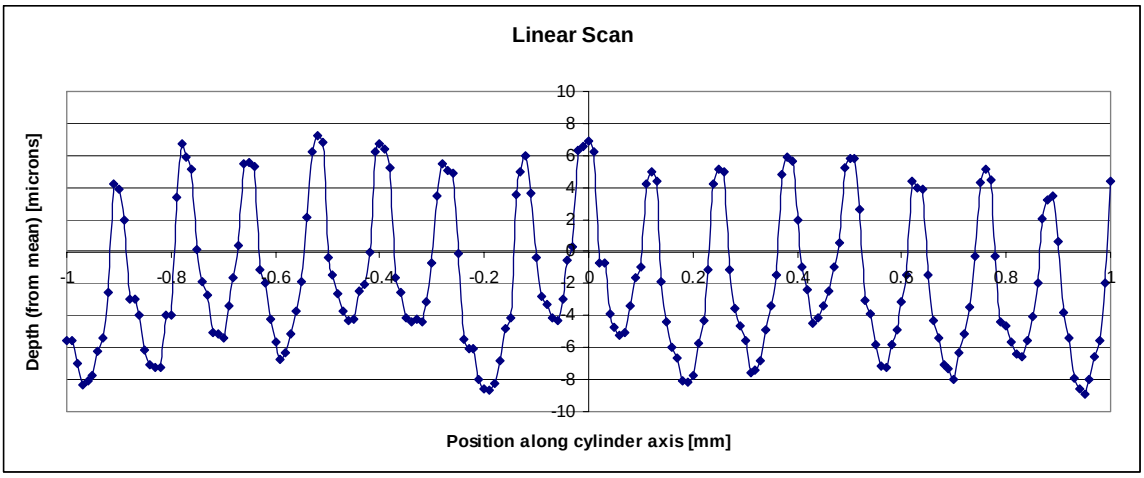

Figure 14: Segment of linear scan along the cylinder axis for fixed angular position. Horizontal scale is mm and vertical scale is microns.

From the specified surface speeds the wavelength of a given tone can be computed for a cylinder. The results are given in Table 4 for a 2 inch cylinder in microns around the circumference. The corresponding angular interval can be scaled from 360° by the circumferential fraction for each tone. Sampling in 0.01^o increments is convenient for the stages and results in a 96 KHz rate for 160 r.p.m.

Table 4: Wavelength for various tones on cylinders for various r.p.m.

diameter (inches)	2.1875				
RPM	80	90	120	144	160
surface velocity (mm/s)	232.740	261.832	349.109	418.931	465.479
frequency	wavelength (μm)				
10	23274.0	26183.2	34910.9	41893.1	46547.9
100	2327.4	2618.3	3491.1	4189.3	4654.8
500	465.5	523.7	698.2	837.9	931.0
1000	232.7	261.8	349.1	418.9	465.5
5000	46.5	52.4	69.8	83.8	93.1
10000	23.3	26.2	34.9	41.9	46.5
15000	15.5	17.5	23.3	27.9	31.0
20000	11.6	13.1	17.5	20.9	23.3
44100	5.3	5.9	7.9	9.5	10.6
88200	2.6	3.0	4.0	4.7	5.3
100000	2.3	2.6	3.5	4.2	4.7

The strategy used was to scan along the axis and then increment the azimuth. At 300 Hz sampling the lateral velocity was therefore the 3 mm/second indicated in Table 2. The data from a segment of one lateral scan is shown in Figure 14. The advantage here is that the data is well organized for the depth determination of each groove at fixed time. The (slight) disadvantage is that the data needs to be reorganized later into a monotonic time series. A time penalty is also incurred (Equation 16) since the linear stage should translate back to the same starting position for each sweep.

The scan executed covered a lateral region of 10 mm length and the full 2π rotation. Approximately 78 grooves were covered in this scan. About 20% of the data set is shown as a surface plot in Figure 15. The vertical scale is exaggerated but a clear deviation from a cylindrical form is seen. The overall deviation is ~250 microns. This can be due to surface imperfections and off-center rotation. The structure is at low frequency since the cylinder rotates at 2.67 Hz during a stylus-based playback, and can be reduced by global fitting, low pass filtering, or other corrections to the data. This is discussed further in Section 4.

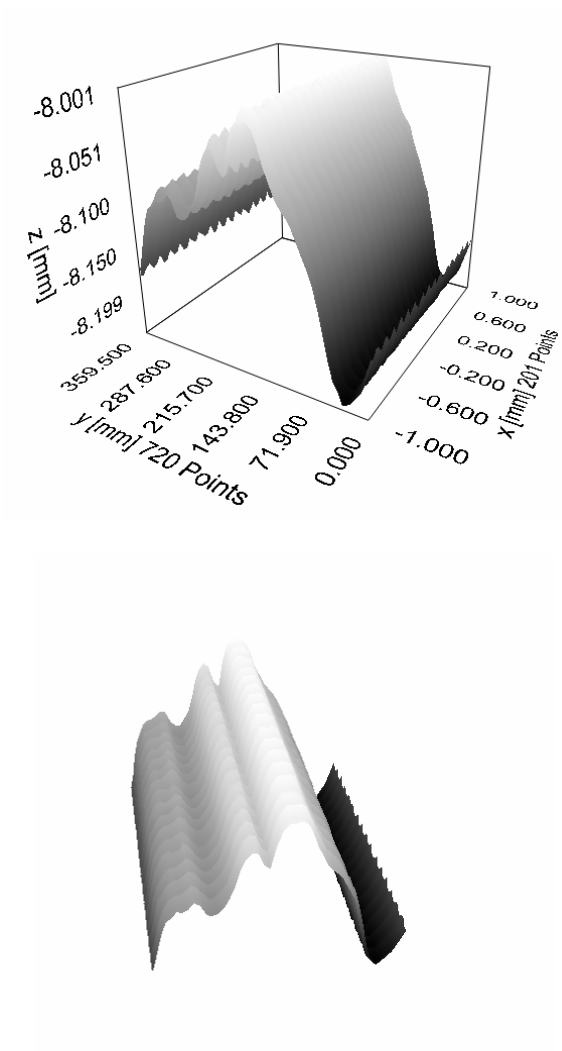

Figure 15: Plots shows 20% of the data scan "unrolled", two views (axes removed on lower view for clarity). Left-right axis (y) is angle from 0 to 360 degrees, axis into the page (x) is position along the cylinder axis in mm, vertical axis (z) is surface height (from a reference point) in mm. A perfect cylinder would be flat at a fixed z position. Instead the surface differs from flat by about 250 microns. This low frequency structure can be due to some combination of shape imperfection, and off-axis rotation.

4. Analysis of Measured Data

As indicated in Section 3, the data scans were taken in slices along the cylinder axis with incremental rotation in azimuthal angle. The grid spacing was 10 μm along the cylinder axis (x). The segment of length 10 mm scanned yielded m=1001 points along the axis. With the azimuthal (ϕ) spacing of 0.01^{o} (5 μm), the full circumference was covered by n=36000 steps. The raw data points consisted of triplets x_{ij}, ϕ_{ij}, *and* h_{ij} (surface height) as follows,

$$\text{data point 1} \;: x_{11}, \phi_{11}, h_{11}$$
$$\text{data point m}: x_{m1}, \phi_{m1,}, h_{m1}$$
$$\text{data point m}+1: x_{12}, \phi_{12,}, h_{12}$$
$$\text{data point m}\times\text{n}: x_{mn}, \phi_{mn}, h_{mn}$$

where for fixed index *i*, x_{ij} is independent of *j* and for fixed index *j*, ϕ_{ij} is independent of *i*. The data were processed as follows.

1. The analysis initially looped over index *i* to find local groove minima (valleys) and maxima (peaks) for each angular slice (fixed index *j*). A segment of one such slice is shown in Figure 14. Slices were then looped over for each angular position *j*.

   1.1. For each angular slice, minima (maxima) candidates were identified as data points which were not higher (lower) than the four nearest points. Some of these candidates can be false or undesirable, due to material damage and extraneous particles (dust or debris).

   1.2. Bad candidate extrema were removed (filtered) using the inherent data periodicity of the known groove structure. The correct groove bottoms (and tops) form a grid with fixed distance between neighbors. For the scanned sample this distance was found to be T = 0.1271 mm, close to expectations for this type of cylinder (200 grooves/inch, see also Table 3). A relative phase, or offset, of the grid along the cylinder length axis was found. For this, a "goodness-of-fit" like quantity was formed,

$$Rsum = \sum_{k=1}^{N} IR(\frac{x[k]}{T} - phase)^2 \qquad (18)$$

   where *IR(y)* is the difference between *y* and the nearest integer value, *N* is the number of extrema in the slice, *k* an index over extrema, and *x*[*k*] the position of the kth extrema along the cylinder axis. This quantity was minimized, with respect to *phase*, to find $Rsum_{min}$ and $phase_{min}$. Then the set of candidates was scanned and the points with

$$IR(\frac{x[k]}{T} - phase_{\min}) > 3.0 \times \sqrt{\frac{Rsum_{\min}}{N}} \qquad (19)$$

   were identified as outliers. They were removed from the list of extrema.

   1.3. The groove ridge heights were taken from the list of maxima identified in the previous step. To find a best estimate for the minimum height the groove shape in the valley is used. For the kth valley, a list of nearby points was formed from the found minimal point and 10 nearest neighbors in the slice. Points were removed from this list if they belonged to the list of maxima or their adjacent neighbor valleys. This set of points was fit to a parabolic function, $H_k(x)$, with a fixed quadratic term using a χ^2 minimization method,

$$H_k(x) = A_k x^2 + B_k x + C_k \qquad (20)$$

$$A_k = \text{constant}$$

$$\chi_k{}^2 = \frac{1}{\sigma^2} \sum_{i=l-5}^{l+5} \left[h_{ij} - H_k(x_{ij}) \right]^2 \qquad (21)$$

where l is the raw data index of the kth valley and j is fixed for the present angular slice. The cutting tools used to imprint the vertical undulations on a particular cylinder are assumed here to have negligible wear over the course of the transcription. Therefore, only the groove position and height will change. The parabolic shape is an approximation to a short circular segment, and is found to fit the local groove shape well. For this sample, the quadratic term was fixed at A = 3.853 mm^{-1}, corresponding to a 130 μm radius for the cutting tool. (By first fitting a large sample of grooves, with no fixed term, this best estimate of the quadratic term was determined.) This value corresponds well to actual historical styli used in recording [X]. The individual point error was assumed to be σ=0.22 μm based upon the width of the distribution of fit residuals. Points were compared to the results of the fit. If an outlying point deviated by more than 3σ, it was removed and the fit was re-iterated. The fit iterations were stopped if no points deviated by more than 3σ or only 5 points remained. As a result of the fit the value of groove position $x_k = -B_k/(2A)$ and depth $d_k = C_k - B_k^2/(4A)$ were obtained. Constraining the data to lie on this parabola is analogous to the simple edge-to-edge distance selection for 2D scanning discussed in the prior work [4].

1.4. The list of fit minima was filtered on the basis of periodicity similar to step 1.2 above. This was done to remove spurious fit results, some of which came from the region near the end of the scan, where the full groove cross-section was not available.

1.5. As described in Section 3, the scan was composed of a set of linear sweeps parallel to the cylinder axis. After each sweep, the probe returned to a starting position. Due to imperfections in the mechanical movement there could be some jitter in the distance between the probe and the cylinder from sweep to sweep. Such "common-mode" offsets were removed by averaging the ~78 ridge maxima across the sweep and subtracting a single number from all fit minima for that sweep. In practice, an average and an r.m.s. value were found, and iterated, to remove outlying maxima beyond 3 time the r.m.s.

2. With a set of groove extrema at fixed azimuth, the data was then re-organized into a time series which followed the spiral trajectory of the groove bottom. This was done by establishing the "seed" groove bottom positions off the first slice. For each position, the groove bottom (ridge) positions in the next slice were searched for in the minimal distance along the cylinder axis. If the minimal distance was less than 30 μm, then the position was attributed to the same groove, and the seed value was updated to that of the next slice. The groove position on the cylinder was traced in this way. As the result of the iterative fitting and periodicity filtering described in steps 1.2 and 1.3, the data would naturally be missing when the groove shape is

corrupted. The distance matching criterion is sufficiently loose to continue tracing the groove in case of missing data

3. The data, fitted and re-ordered, should contain 36,000 points per cylinder rotation, corresponding to the 96 KHz sampling for the 160 r.p.m. sample. Any missing points, due to the cuts discussed above, are linearly interpolated from the neighboring points. At least three data streams can be derived from this set.

   3.1. The groove bottoms can be considered as a stand-alone data stream.
   3.2. The groove top (ridges) can be considered as a stand-alone data stream.
   3.3. The groove bottom position can be considered with respect to the top position. In this way the local surface imperfections seen in Figure 15 can be subtracted out. The groove top can be used to track the generic cylinder surface shape. The groove top determination for a given slice is less precise than the bottom, because less measurement points went into its height value, and because of potentially more wear. Therefore, a point-by-point bottom-top subtraction would add noise. Instead a low sampling frequency template was made by averaging every 100 top points corresponding to one degree of azimuthal angle. Each bottom height value was referenced to a parabolic interpolation of the local top value taken from three nearest points of the top template. Due to the low sampling frequency of the template, the correction for the surface irregularity was restricted to low frequencies.

4. Excess frequency content was filtered using a Discrete Fourier Transform (DFT) method, implemented as a Fast Fourier Transform (FFT). This was done both to satisfy the Nyquist criteria before re-sampling to a lower frequency digital audio rate and because the recorded cylinder and acoustic horn technology has only a limited frequency content as discussed in Section 2. In addition, the sound amplitude is proportional to the stylus velocity, rather than displacement. The measured groove depth distribution is therefore differentiated to determine the stylus velocity. The filtering and differentiation can be accomplished in single step using the DFT as follows. Define $A(nT)$ as the unfiltered waveform in the time domain and $C(k)$ as the kth element of its DFT, where k is the harmonic number, $n=n^{th}$ time sample, and T=sampling period. Define $A_F(nT)$ to be the filtered form of $A(nT)$. The total number of samples is N, and $2\pi f=k\Omega$, where f is the frequency in cycles per second. Let M(k) be an imposed filtering function. As equation (22) shows, filtering and differentiation is caused by the $(-ik\Omega)M(k)$ multiplier applied to the DFT coefficients.

$$\frac{d}{d(nT)}A_F(nT) = \frac{d}{d(nT)}F_D^{-1}[C(k)] = \frac{1}{N}\sum_{k=0}^{N-1}\frac{d}{d(nT)}M(k)C(k)e^{-ik\Omega nT}$$
$$= \frac{1}{N}\sum_{k=0}^{N-1}(-ik\Omega)M(k)C(k)e^{-ik\Omega nT} \qquad (22)$$

The filtering factor M is defined as follows.

$$M = \begin{cases} 0 \ \ for \ \ f < 20Hz \\ 1 \ \ for \ \ f \in [20Hz, 4.8KHz] \\ \left(1.0 - \dfrac{(f - 4.8)}{0.4}\right) \ \ for \ \ f \in [4.8KHz, 5.2KHz] \\ 0 \ \ for \ \ f > 5.2 \ KHz \end{cases} \qquad (23)$$

4.1. The cut below 20 Hz removes the low frequency structure in the bottom-only data due to the cylinder shape irregularity.
4.2. The 400 Hz wide transition to zero at 5.0 KHz was used to avoid the interference-like pattern triggered by jumps in the data.
4.3. The cut above 5.2 KHz satisfies the Nyquist criteria before re-sampling to a lower digital audio standard.

All the data from the scanned sample could not be easily processed simultaneously, due its size. Instead, one second long samples were treated sequentially. The filtering was done in 100,000 points space, of which 96000 points corresponded to the scanned sampling frequency. Two “zero-padding” regions of 1000 points lengths were placed before and after each such chunk of data, with the same length linear transitional regions in between. This was done to avoid mismatching jumps between sequential samples.

5. The list of filtered height measurements was rescaled to 16 bit dynamic range, and converted to WAV format with 22.05 KHz sampling.

The audio data is shown in Figure 16a, b, and c for the three streams described in Step 3 above and can be accessed at an Internet URL [32]. Note the scale differences in the figures. Interestingly, the groove top stand-alone stream contains audible, albeit noisy sound, with some interference from different times in the recording. This may be due to the residual localized pressing of the carving tool on the nearby surface. The pressing on the two grooves on both sides of a ridge can create the mentioned interference.

Because of the sound content in the top stream, and the possibility of some “self-subtraction’, the top/bottom subtracted method is not free of bias. Due to the logarithmic perception of the sound amplitudes, the amplitudes in samples would have to be very close for the audible degradation to occur and as practical matter there is, however, little effect. The implicit correction for global cylinder shape is valuable and therefore this approach is shown as well. It effectively removes structures below about 100 Hz which are in-fact only marginally audible.

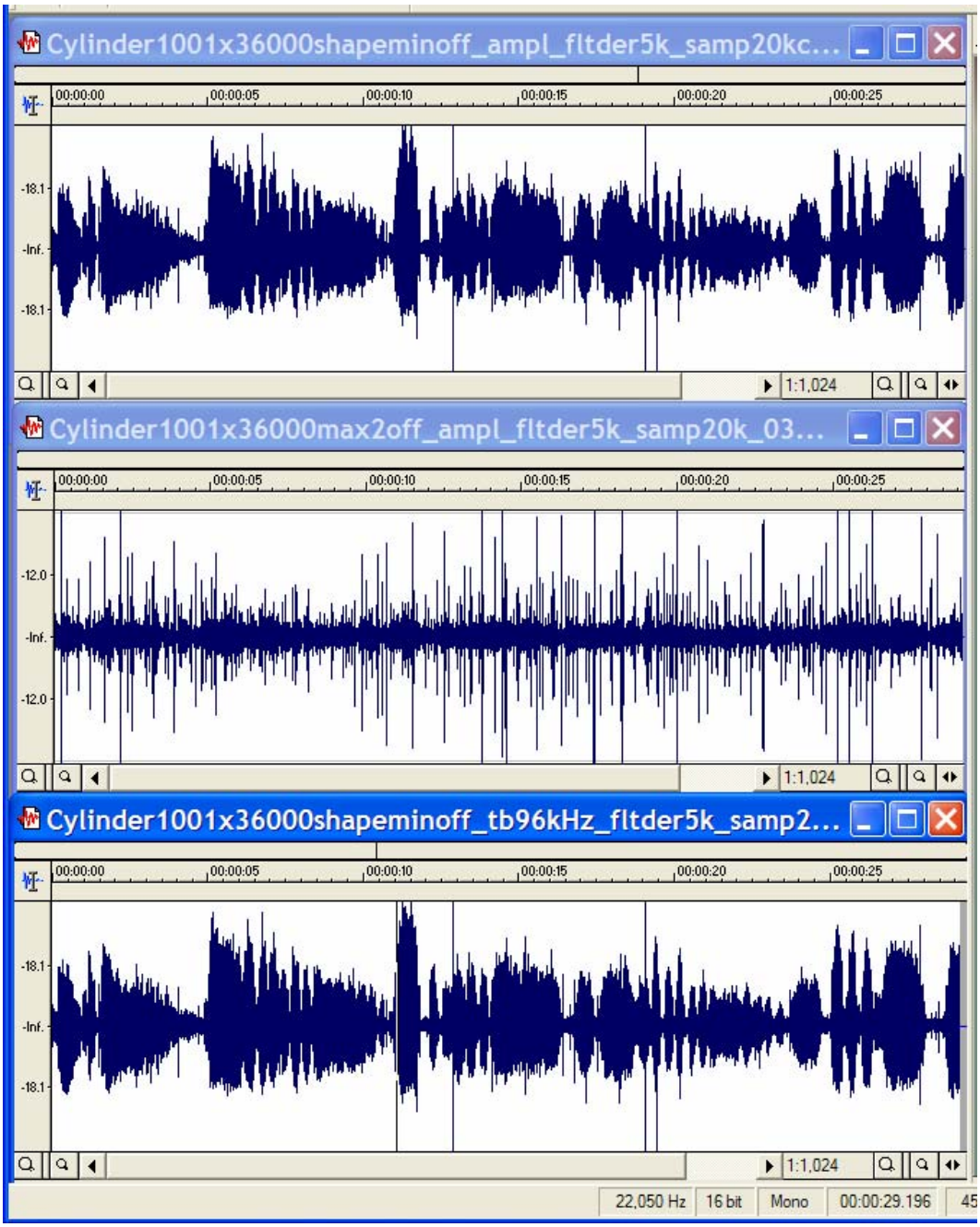

Figure 16: a) top shows audio stream from bottom only extraction, b) middle shows audio stream from ridge top only extraction, and c) lower shows top-bottom extraction.

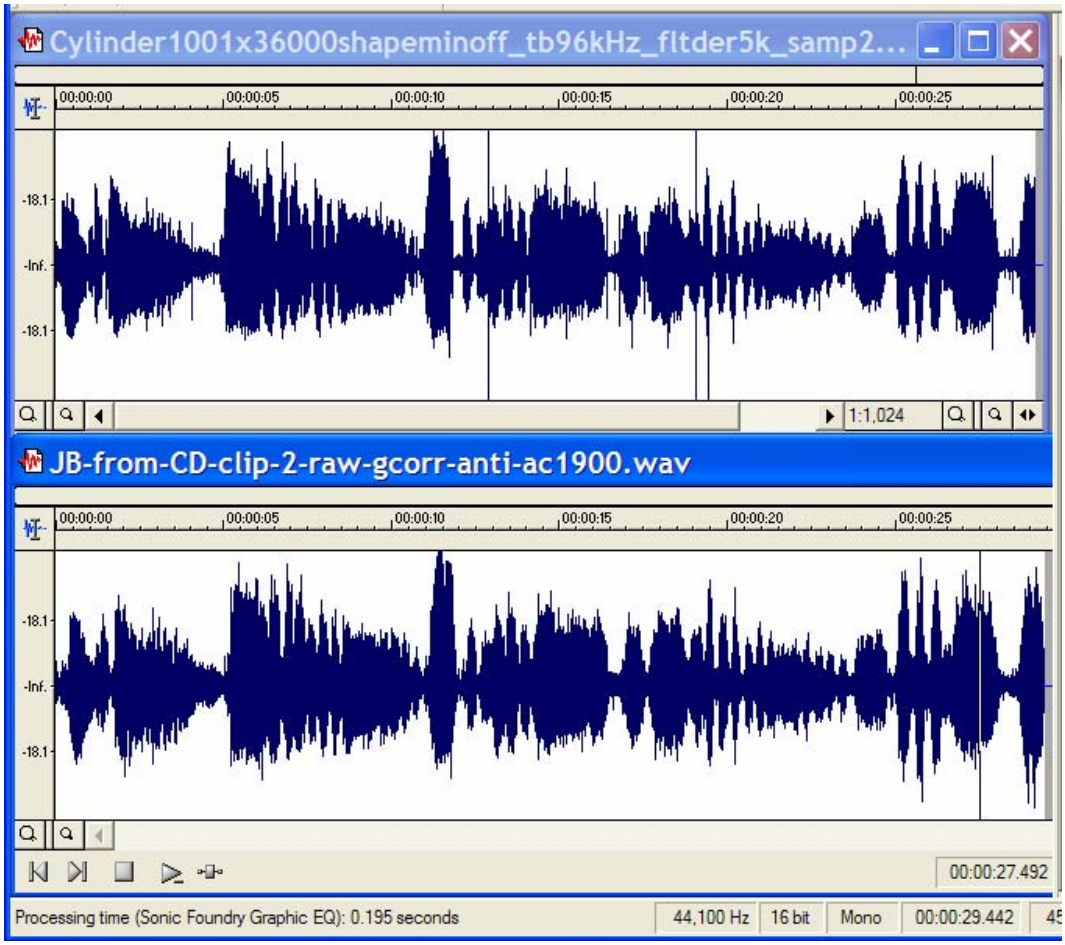

Figure 17: a) top shows top-bottom audio extraction, identical to Figure 16c and b) lower shows stylus playback of the same source material with no additional processing applied. Approximately 29 seconds on audio is shown. Line structure seen at 27.492 seconds in b) is a cursor. We attribute the slight time scale difference to the cylinder rotation speed accuracy in the stylus-based playback.

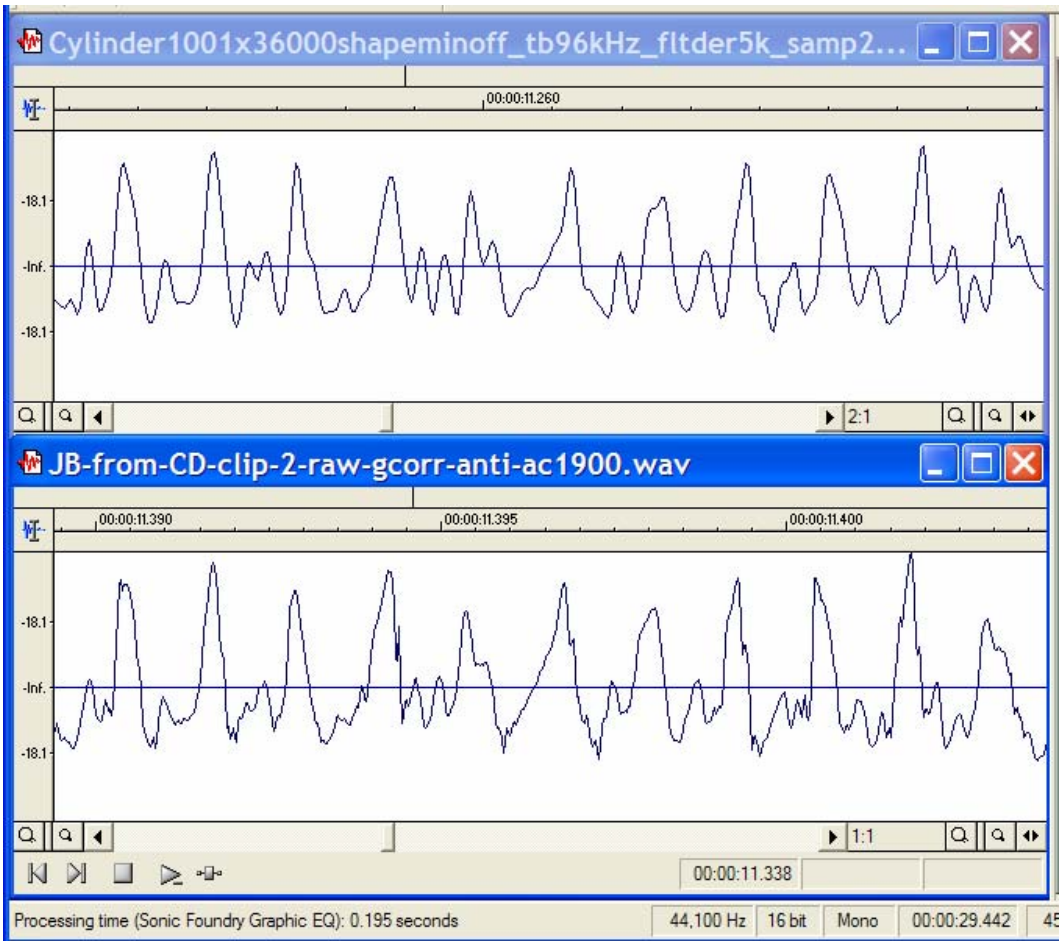

Figure 18: a) top is the same data as Figure 17a but expanded to show a segment of length 14 milliseconds beginning at 11.254 seconds from the start of the clip, b) bottom is the corresponding section from the stylus version.

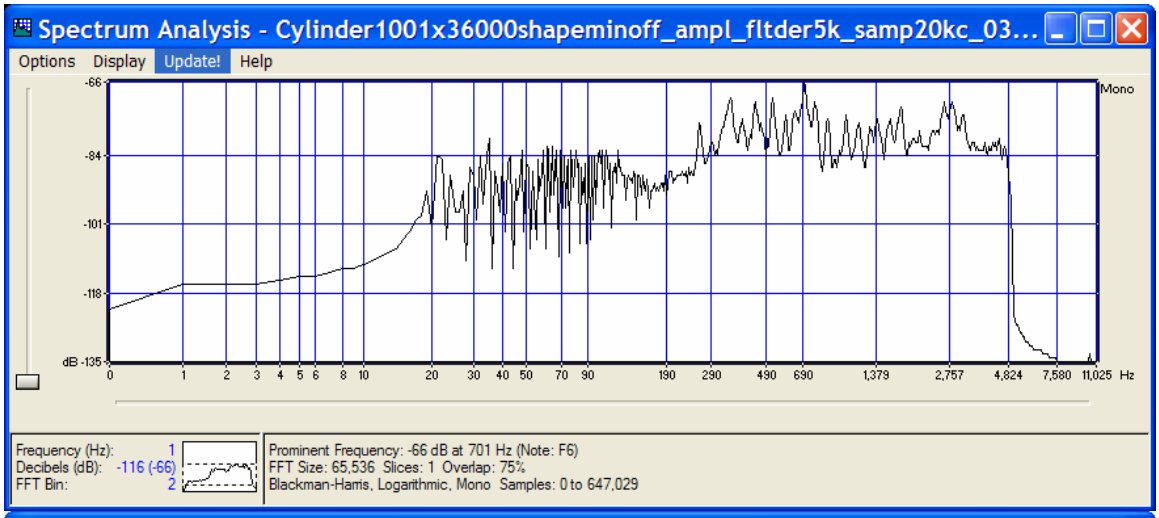
Spectrum Analysis - Cylinder1001x36000shapeminoff_ampl_fltder5k_samp20kc_03...
Options Display Update! Help
Mono
-66
-84
-101
-118
dB -135
0 1 2 3 4 5 6 8 10 20 30 40 50 70 90 190 290 490 690 1,379 2,757 4,824 7,580 11,025 Hz
Frequency (Hz): 1
Decibels (dB): -116 (-66)
FFT Bin: 2
Prominent Frequency: -66 dB at 701 Hz (Note: F6)
FFT Size: 65,536 Slices: 1 Overlap: 75%
Blackman-Harris, Logarithmic, Mono Samples: 0 to 647,029

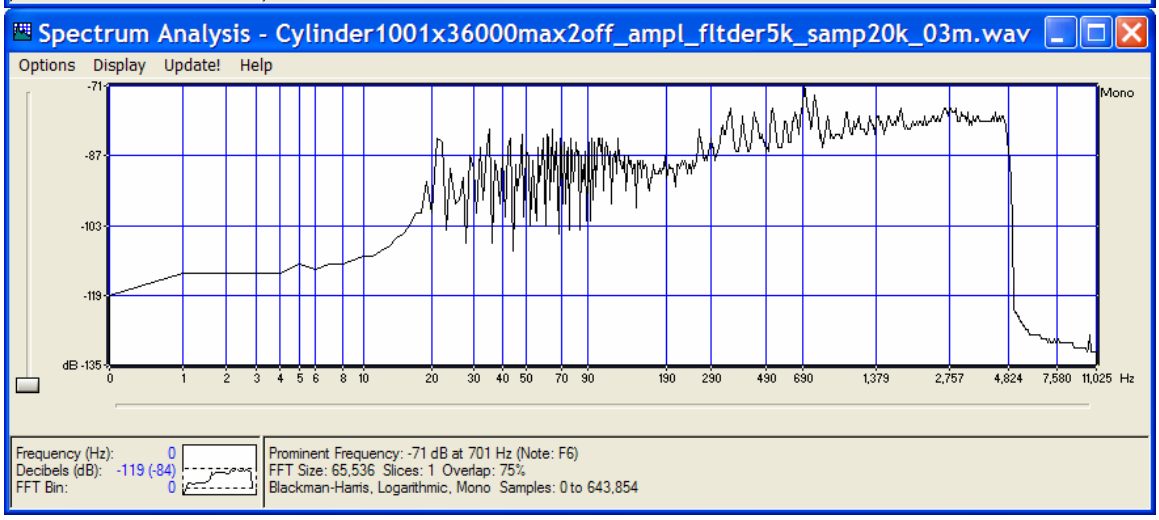
Spectrum Analysis - Cylinder1001x36000max2off_ampl_fltder5k_samp20k_03m.wav
Options Display Update! Help
Mono
-71
-87
-103
-119
dB -135
0 1 2 3 4 5 6 8 10 20 30 40 50 70 90 190 290 490 690 1,379 2,757 4,824 7,580 11,025 Hz
Frequency (Hz): 0
Decibels (dB): -119 (-84)
FFT Bin: 0
Prominent Frequency: -71 dB at 701 Hz (Note: F6)
FFT Size: 65,536 Slices: 1 Overlap: 75%
Blackman-Harris, Logarithmic, Mono Samples: 0 to 643,854

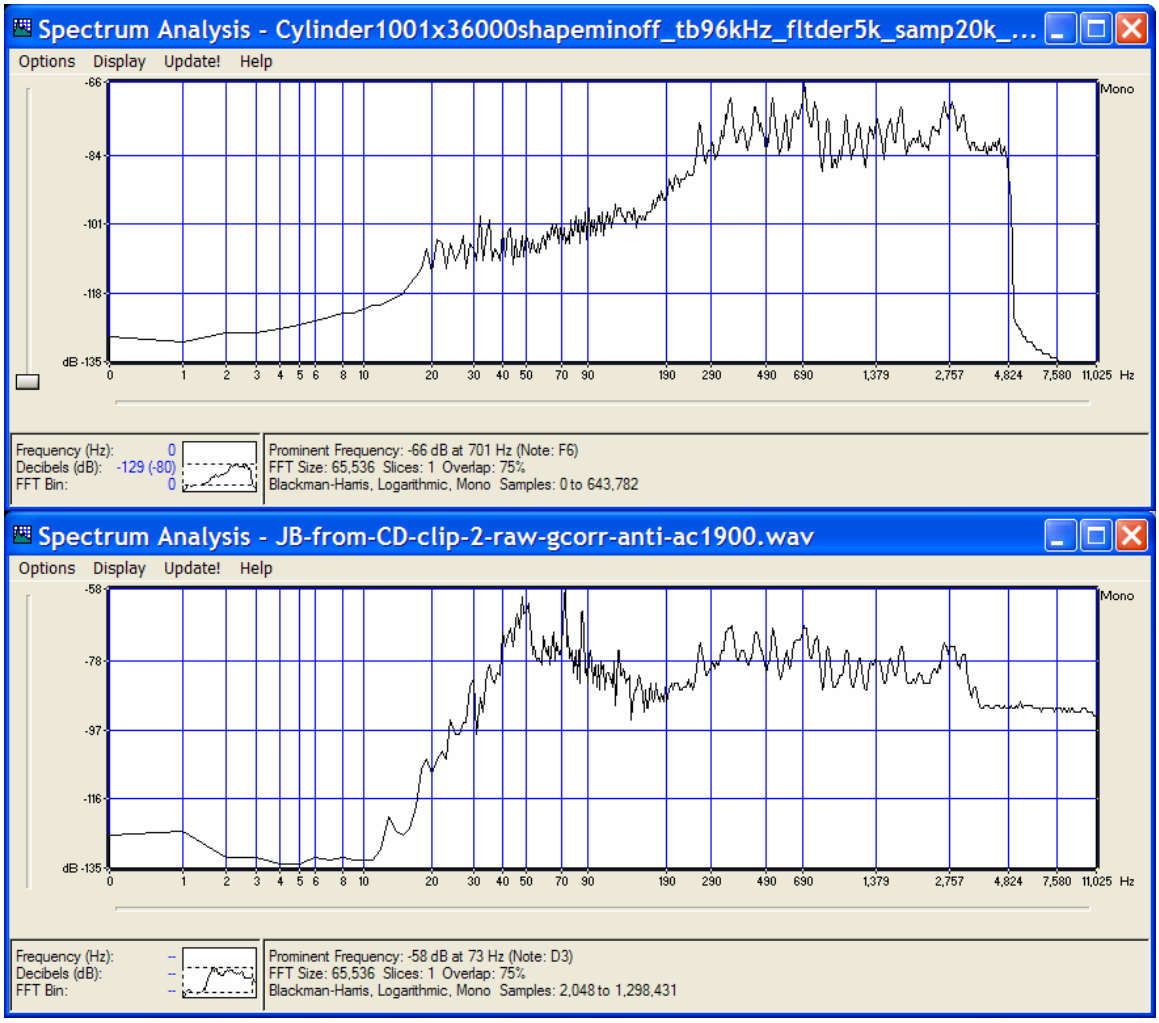

Figure 19 a) top Fast Fourier Transform spectrum analysis of data of Figure 16a groove bottom only, b) FFT of top ridges only as in Figure 16b, c) FFT of top-bottom subtracted data, and d) FFT spectrum analysis of stylus playback data of Figure 17b.

To make a comparison with stylus playback, a commercial re-issue of this same source material was obtained from Archeophone Records Inc. The producer provided a raw transcription without any post-processing although a known bass boost had been applied [33]. The comparison is shown in Figure 17a and b for the optical and raw stylus versions respectively. The bass boost has been removed from the stylus version. Figures 18a and b show an expanded view of these same clips. This sample is available at the aforementioned URL as well.

As shown in Figures 16 and 17, the bottom-only and bottom/top subtracted samples are indeed very similar and also similar to the stylus versions. However, the bottom-only sample has a some periodic clicking sound content, similar to a stylus striking an obstacle. This feature is similar to what can be heard more clearly on the “raw” sound from the stylus playback and may therefore be inherent to this recording. The comparison is also illustrated in Figure 19a-d which show FFT spectrum analysis for the

bottom-only, top, bottom/top, and stylus versions respectively. From these it is clear that the stylus version contains significantly more low frequency artifacts.

5. Discussion

It is clear from the figures and clips that the 3D optical method provides an accurate audio transcription as compared to a stylus playback. There are a number of issues for further consideration.

No post-processing has been applied to the samples presented here. In principle the sound quality could be enhanced by additional bass boost, and digital de-clicking or noise reduction.

An example of a damage site is shown in Figure 20. This figure illustrates that damage structures can be of significant size compared to the characteristic amplitudes of the cylinder technology. The fixed grid, time-slice-based approach, while simple to implement, and effective in the noise reduction when used in shape-based filtering, may not be optimal for certain complex damage sites. For those, the full 3D data should be used to “delete” or correct the damage site. The adjacent undamaged regions would be used as a basis for such an interpolation which may be statistically determined. A denser sampling of the surface may be required to fully correct the “clicks” and “pops” which manage to pass the initial filtering procedure. This could be accomplished by returning to damage sites after an initial scan and re-measuring with a finer grid. The usefulness of this approach could be the topic of a subsequent study.

Another related area concerns samples with surface contamination. An important example is brown or white mold which is known to grow on the surface of wax cylinders. Due to the inherent multiple sampling across the groove profile in this method, it may be possible to overcome these effects at some level. Again, the grid density is a variable which may require further optimization. If the mold is known to always be additive or subtractive of the surface a shape fitting constraint could be developed.

In Section 2 the aliasing issues were discussed. From the results presented, it seems unlikely that a significant aliased signal is folded into the audible region. As a further demonstration of this, Figure 21 shows an FFT spectrum of the data at the raw 96 KHz sampling, before any differentiation, filtering, or re-sampling has been applied. Any noise content above 48 KHz should be a continuation of the level present just below 48 KHz, or if it is already aliased, then less. The level seen is already a sizable factor below the signal baseline in the audible region. These issues could be explored further with more complex optical sampling strategies as discussed in Section 2.

A clear area for improvement is in scan time. A subsequent study could consider the effect of a coarser baseline grid on signal quality. Such an approach could yield significant improvements in scan time. Confocal probes can also run at faster sampling rates than the 300 Hz applied here, at some potential loss of reflected signal.

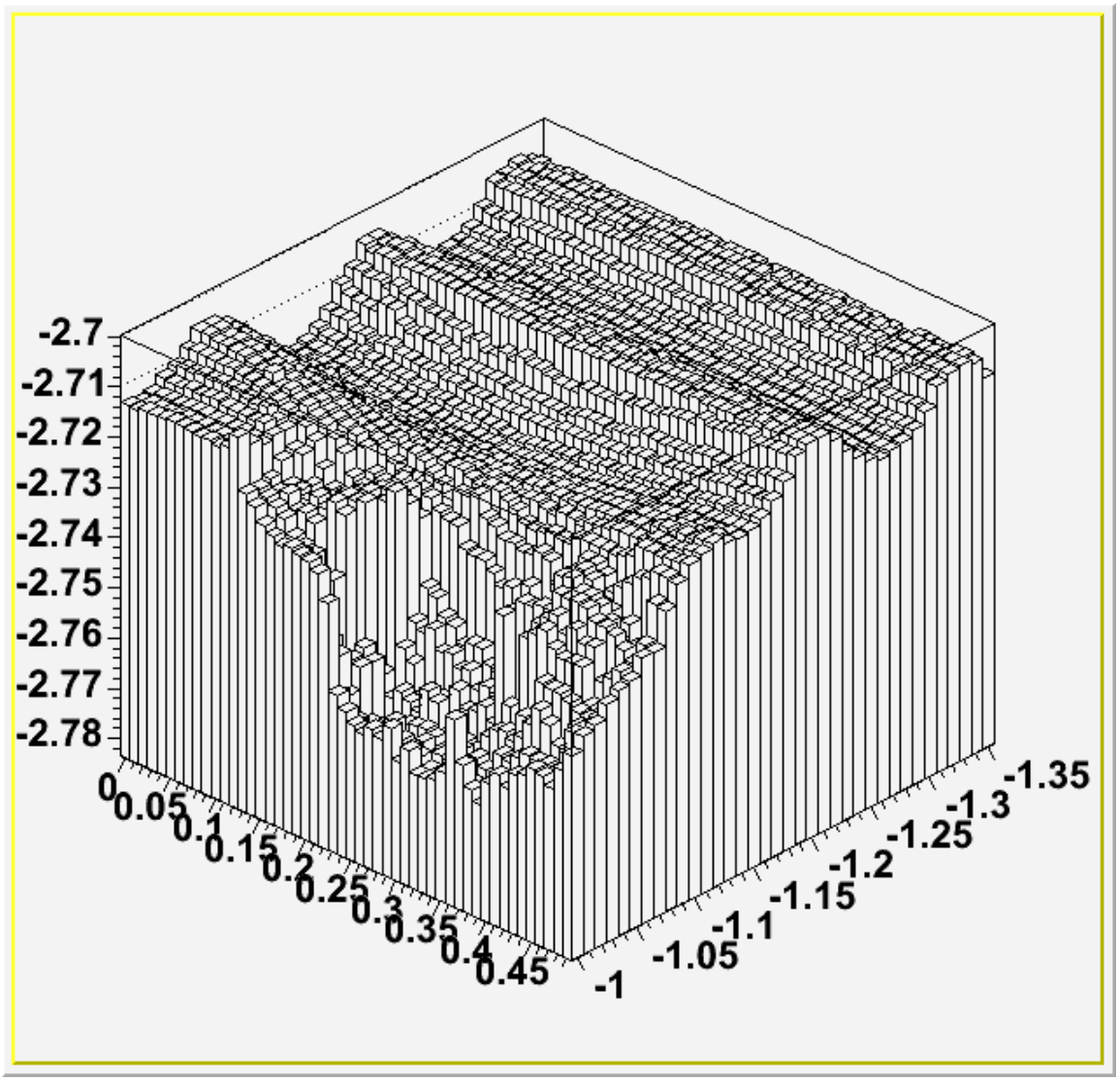

Figure 20: Example of a damage site on the cylinder. Scale is in millimeters. Each 2D bin represents a measurement point of size 5 microns along the groove and 10 microns across the groove.

6. Conclusions

The technical basis for 3D surface metrology applied to audio recovery from mechanical media has been discussed. A proof-of-principle was demonstrated on a celluloid cylinder and results were comparable to stylus playback. Further development of these methods could enable the systematic recovery of delicate, damaged, broken, or moldy samples. Optimized hardware, software, and analysis tools could further enhance the impact of these methods on audio preservation.

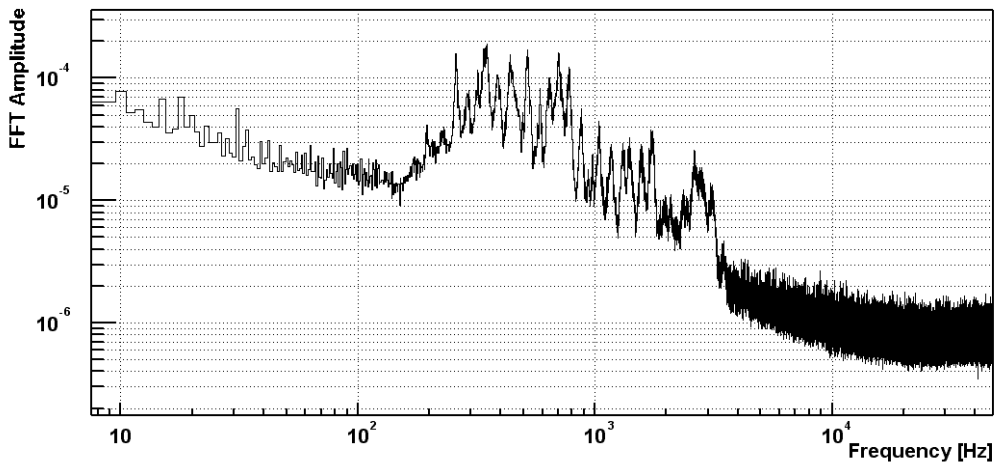

Figure 21: The FFT spectra of the reconstructed sample groove amplitudes before differentiation. For the initial sampling at 96 KHz, the Nyquist frequency is 48 KHz. Any noise which is aliased to lower frequency is below the baseline noise at audible frequency.

Acknowledgements

This work was supported by the Laboratory Technology Research Program (SC-32), within the Office of Science, U.S. Department of Energy under Contract No.DE-AC03-76SF00098.

The authors wish to thank and acknowledge a number of individuals for assistance in this work. Bill Klinger and Sam Teicher provided advice and cylinder samples. Richard Martin and Meagan Hennessey of Archeophone Records provided stylus transcriptions of source material. Mark Roosa, Peter Alyea, Lawrence Appelbaum, and Samuel Brylawski, of the Library of Congress provided advice, encouragement, and samples. Peter Copeland offered interesting remarks on the aliasing issues. George Horn of Fantasy Records in Berkeley, California critiqued the sound quality and offered valuable advice on equalization. Gerald Fabris of the Edison National Historic Site provided information on horn geometries used in the acoustic era. Roger Waxler provided comments and insight into the physics of sound propagation and horns.

Sample scans were provided by STIL SA (Aix en Provence, France), Veeco Instruments Incorporated (Tuscon, Arizona), and Microphotonics Incorporated (Irvine, California). The authors wish to acknowledge the assistance of the staff at each of these companies.

Appendix

The known parameters of mechanical recordings, as determined from a number of sources [23-26] are tabulated here. Figures 6 and 7 relate these parameters to the configuration of grooves on cylindrical and disc media respectively. When relevant they are defined at a specific frequency (1000 Hz) where equalization is generally not applied.

1) Groove width: distance across the top of the groove.
2) Grooves per inch (G_d): the number of grooves cut in the surface per radial inch.
3) Groove spacing: center to center distance between two adjacent grooves.
4) Fixed Groove Depth: for a lateral disc recording, the depth of the groove below the surface. Not applicable to vertical cut recordings.
5) Reference signal level: the peak transverse velocity used to set a baseline for the recorded signal. This quantity is in principle arbitrary but is key to defining the noise and dynamic range discussed in the literature.
6) Maximum groove amplitude: the maximum displacement of the groove from an un-modulated path.
7) Noise level below reference level (signal to noise ratio): noise levels or limits are usually expressed as dB below the reference signal. This is taken to mean the standard deviation of any random noise source, such as the underlying surface noise source discussed above, or the maximum allowed deviations due to the low frequency systematic effects.
8) Dynamic range: a measure of the range of audible signals up to the maximum peak recorded signal level, defined here with respect to the noise level at 1000 Hz
9) Groove amplitude at noise level: maximum amplitude deviation from a signal free path corresponding to the noise level in item 6) above and defined in equation 2.
10) Maximum and minimum radii: the respective radii at which audio data is specified to begin (R_{MAX}) and end (R_{MIN}).
11) Area: the area covered by audio data. For a cylinder L is the length along the axis.

$$Area = \pi(R_{MAX}^2 - R_{MIN}^2) \quad \text{disc} \qquad \text{(A - 1)}$$

$$Area = 2\pi R\text{L} \quad \text{cylinder} \qquad \text{(A - 2)}$$

12) Total length: the path length along a complete groove between the two radial extremes.

$$L = G_d \times Area \qquad \text{(A - 3)}$$

Table A1: Parameters of grooves on different mechanical media.

Parameter	**Coarse**	**Micro-Groove**	**Cylinder**
Diameter inches	10-12	12	2-5
Revolutions per minute	78.26	33.3333	80-160
Groove width at top	150-200 μm	25-75 μm	variable
Grooves/inch G_d (mm)	96-136 (3.78-5.35)	200-300 (7.87-11.81)	100-200 (3.94-7.87)
Groove spacing	175-250 μm	84-125 μm	125-250 μm
Fixed Groove depth	40-80 μm	25-32 μm	NA
Ref level peak velocity@1KHz	7 cm/s	7 cm/s (11 μm)	unknown
Maximum groove amplitude	100-125 μm	38-50 μm	~10 μm
Noise level below ref, S/N	17-37 dB	50 dB	unknown
Dynamic range	30-50 dB	56 dB	unknown
Groove max ampl@noise level	1.6 - 0.16 μm	0.035 μm	< 1 μm
Max/Min radii mm	120.65/47.63	146.05/60.33	fixed
Area containing audio data	38600 mm^2	55650 mm^2	16200 mm^2 (2’’)
Total length of groove meters	152	437	64-128

.

Disclaimer

This document was prepared as an account of work sponsored by the United States Government. While this document is believed to contain correct information, neither the United States Government nor any agency thereof, nor The Regents of the University of California, nor any of their employees, makes any warranty, express or implied, or assumes any legal responsibility for the accuracy, completeness, or usefulness of any information, apparatus, product, or process disclosed, or represents that its use would not infringe privately owned rights. Reference herein to any specific commercial product, process, or service by its trade name, trademark, manufacturer, or otherwise, does not necessarily constitute or imply its endorsement, recommendation, or favoring by the United States Government or any agency thereof, or The Regents of the University of California. The views and opinions of authors expressed herein do not necessarily state or reflect those of the United States Government or any agency thereof or The Regents of the University of California.

References

[1] Hart, M., **J.Audio Eng. Soc**, Vol. 49, No. 7/8,2001 July/Aug

[2] **Folk Heritage Collections in Crisis,** published by The Council on Library and Information Resources, 1996, ISBN 1-887334-82-3

[3] Fox, Barry, “Not Fade Away”, **New Scientist**, 1st March 2003, pp 40-43

[4] Fadeyev V. and Haber, C., **J. Audio Eng. Soc**., vol. 51, no. 12, pp. 1172-1185 (2003 Dec.).

[5] Fremer, M., "Analog Corner", **Stereophile**, December 2003

[6] T. Iwai, T. et al., **Appl. Opt.,** vol. 2, no.5, (1986) pp. 597-604

[7] Penn, W. and Hanson, M.J., "The Syracuse University Library *Radius Project:* Development of a non-destructive playback system for cylinder recordings" **First Monday**, volume 8, number 5 (May 2003)

[8] Poliak, J., Robert, P., and Goy, J., Optical Fibre Turntable for Archive Records, **Proceedings of the 92nd Convention AES**, Vienna, Austria.

[9] Petrov, V.V., et al., "Optomechanical method of Edison cylinders sound reproduction" **Audio Eng. Soc. Preprint** (Preprint 4491), Munich 1997, March 1997

[10] Cavaglieri, S., Johnsen, O., and Bapst, F., **Proc of AES 20th International Conference**, Budapest, Hungary 2001, Oct 5-7.

[11] Stanke, G. and Paul, L., **Inform. Serv. & Use,** 15 (1995) pp. 289-301

[12] Powell, J. R. and Stehel, R. G., **Playback Equalizer Settings for 78 RPM Recordings,** Grammaphone Adventures, 1993

[13] Morse, P.M., **Vibration and Sound**, 1st Edition, McGraw-Hill, 1936

[14] Morse, P.M., **Vibration and Sound**, 2nd Edition, McGraw-Hill, 1948

[15] Molloy, C.T., **J. Acoust. Soc. Am.,** 22:551-557 (1950)

[16] Blackstock, D.T., **Fundamentals of Physical Acoustics**, Wiley-Interscience, 2000

[17] Olson, H.F., **Acoustical Engineering**, Van Nostrand, 1957

[18] Pierce, A.D., **Acoustics,** McGraw-Hill, 1981

[19] Maxfield, J.P. and Harrison, H.C., **The Bell System Technical Journal**, Volume V, No.3, July 1926, pp. 493-524

[20] The data plotted in Figure 4 was first published by Maxfield and Harrison [20] and subsequently re-plotted by Olson [17]. Olson's plot is shown here. However Olson claims the response shown is for a recording with a low frequency attenuation of 6 dB/octave below 800 Hz. Comparing this plot to the original in reference [19], the present authors cannot see how Olson's claim is born out. In either case the cut-off frequencies are not affected, only the shape from cut-off to 800 Hz.

[21] Webster, A.G., **Proc. Nat. Acad. Sci. of the U.S.A.**, No. 7, July 15, 1919, pp. 275-282

[22] George Horn, private communication, emphasized the apparent attenuation of low frequency content in these recordings.

[23] EIA Specification RS-211-Rev D and Rev C.

[24] Read, Oliver, **The Recording and Reproduction of Sound**, H.Sams, 1953

[25] Langford-Smith, F., editor, **Radiotron Designer's Handbook**, Fourth Edition. The Wireless Press, 1953.

[26] Certain cylinder recording parameters were provided by Bill Klinger of the Association of Recorded Sound Archives (ARSC), private communication

[27] Corle, T.R., and Kino, G.S., **Confocal Scanning Optical Microscopy and Related Imaging Systems,** Academic Press, 1996

[28] Cohen-Saban, J. et al, **Proc. SPIE**, 4449, 178-183, (2001)

[29] Davidson, M. et al, **Proc. SPIE**, 775, 233-247, 1987

[30] Caber, P.J., **Applied Optics** 32, 3438-3441 (1993)

[31] Klinger, B., "**Stylus Shapes and Sizes: Preliminary Comments on Historical Edison Cylinder Styli**", Association for Recorded Sound Collections Report, 2004

[32] The audio clips can be accessed at http://www-cdf.lbl.gov/~rnd/ (temporary site), permanent site will be http://www-cdf.lbl.gov/~av/

[33] Kevin Barrett, private communication, the pre-amplifier used was the VSP Souvenir from KAB Electro-Acoustics, with the AC 1900 equalization defined as follows: bass boost at 3dB/octave, +3dB point is 500 Hz, maximum boost is +10dB; treble roll-off is -3dB/octave, -3dB point is 5000 Hz.